PCCP

PAPER

View Article Online
View Journal | View Issue

Cite this: *Phys. Chem. Chem. Phys.*, 2018, **20**, 25780

Hydration of 3-hydroxy-4,4-dimethylglutaric acid with dimethylamine complex and its atmospheric implications†

Ya-Juan Han,[ab] Ya-Juan Feng,[c] Shou-Kui Miao,[ac] Shuai Jiang,[c] Yi-Rong Liu,[c] Chun-Yu Wang,[ac] Jiao Chen,[d] Zhong-Quan Wang,[ac] Teng Huang,[a] Jie Li[c] and Wei Huang *[ace]

Received 25th June 2018,
Accepted 19th September 2018

DOI: 10.1039/c8cp04029j

rsc.li/pccp

Atmospheric aerosols have a tremendous influence on visibility, climate, and human health. New particle formation (NPF) is a crucial source of atmospheric aerosols. At present, certain field observations and experiments have discovered the presence of 3-hydroxy-4,4-dimethylglutaric acid (HDMGA), which may participate in NPF events. However, the nucleation mechanism of HDMGA has not been clearly understood. In addition, dimethylamine (DMA) is an important precursor of nucleation. The nucleation mechanism involving HDMGA and DMA has not been studied. In this study, the most stable structures of (HDMGA)$(H_2O)_n$ (n = 0–3) and (HDMGA)(DMA)$(H_2O)_n$ (n = 0–3) were obtained by using M06-2X coupled with the 6-311++G(3df,3pd) basis set. The α-carboxyl group is directly attached to the amino group in all the most stable configurations. Proton transfer enhances the strength of a hydrogen bond, as well as promotes the generation of a global minimum structure. Temperature has a considerable influence on the distribution of isomers for (HDMGA)(DMA)$(H_2O)_3$ as compared to the other investigated clusters. The Gibbs free energy values reveal that most of the clusters can exist in NPF, except for (HDMGA)$(H_2O)_1$. The process of adding a cluster of $(H_2O)_n$ more likely occurs in the atmosphere than gradually adding a single water molecule.

1. Introduction

Atmospheric aerosols, which are formed by suspended solid or liquid small particles in gaseous media, have a tremendous impact on Earth's climate, human health, and so on.[1–4] The scattering and absorption of solar radiation reduce atmospheric visibility and change the balance of solar radiation, which is a direct environmental impact of atmospheric aerosols.[1,4] New particle formation (NPF) through gas-to-particle transformation contributes toward an increase in the number of aerosol particles, which is more than half of the cloud condensation nuclei (CCN).[2,5,6] NPF comprises two processes:[7–10] forming a critical nucleus and further growth of this critical nucleus.[9,11] The first step of nucleation is vital because the critical nucleus may affect the population and nucleation rate. Even though the nucleation mechanisms have been investigated since a long time, the precise chemical compounds and procedures at the molecular cluster level have several uncertainties.[9,12] It is difficult to understand the nucleation events in the ocean area by the binary homogeneous nucleation of sulfuric acid and water, suggesting that other atmospheric components may be involved in the nucleation process.[9,12,13]

The formation of atmospheric aerosols is partly because of biological and anthropogenic sources. Primary aerosols are pollutants, which are directly released into the atmosphere; secondary organic aerosols (SOA) are generated through the oxidation of anthropogenic and biogenic volatile organic compounds (VOCs) with oxidants like nitrogen oxides (NO_x), ozone (O_3), and OH radicals.[14–17] SOA, as an important part of atmospheric aerosols, account for about 20–80% of the overall organic aerosol mass.[18] Biogenic VOCs (BVOCs), mainly including isoprene (C_5H_8) and monoterpene ($C_{10}H_{16}$), are primary global SOA precursors rather than anthropogenic VOCs.[19,20] Previous studies have revealed that global terpene emissions are approximately 120–480 Tg y^{-1},[19] which is larger than global

[a] *Laboratory of Atmospheric Physico-Chemistry, Anhui Institute of Optics & Fine Mechanics, Chinese Academy of Sciences, Hefei, Anhui 230031, China*
[b] *School of Environmental Science & Optoelectronic Technology, University of Science and Technology of China, Hefei, Anhui 230026, China*
[c] *School of Information Science and Technology, University of Science and Technology of China, Hefei, Anhui 230026, China. E-mail: huangwei6@ustc.edu.cn*
[d] *Anhui Branch of China Meteorological Administration Training Center, Hefei, Anhui 230031, China*
[e] *Center for Excellent in Urban Atmospheric Environment, Institute of Urban Environment, Chinese Academy of Sciences, Xiamen, Fujian 361021, China*

† Electronic supplementary information (ESI) available. See DOI: 10.1039/c8cp04029j

anthropogenic VOCs emissions (100 Tg y^{-1}).[21] Some researchers have indicated that the emission factor of monoterpenes is much lower than that of isoprene;[19,22] however, the SOA yield of monoterpenes is 16 times that of isoprene.[23] In Hong Kong,[24] the US,[25,26] and the Arctic region,[27] the predominant SOA precursors were monoterpenes. Monoterpenes—a kind of BVOC—can be oxidized into SOA *via* different oxidants, such as NO_x, O_3, and OH radicals.[28,29] The estimated annual global emission rate of monoterpenes is about 127 Tg, the main contributor being conifers with α-pinene.[19] Different SOA tracers can facilitate researchers to understand the formation processes of SOA and acquire important information about precursors.[15,24,27,30–32] Organic species, such as monoterpene SOA tracers, namely, *cis*-pinonic acid and pinic acid, form an important part of newly formed particles (3–5 nm in diameter).[33] In a recent study, M. Claeys *et al.*[16] found a novel compound in two different places, namely, (1) 3-hydroxy-4,4-dimethylglutaric acid as the α-pinene tracer with the chemical characteristics of trifunctional hydroxy dicarboxylic acids in $PM_{2.5}$ (fine particulate matter) field samples with mixed deciduous and coniferous vegetation and (2) in an irradiated α-pinene/NO_x smog chamber. $PM_{2.5}$[34] refers to particles with aerodynamic diameters equal to or less than 2.5 μm. Later, it was found again over oceans from the Arctic to the Antarctic.[35] The abbreviation of 3-hydroxy-4,4-dimethylglutaric acid is HDMGA. In view of the trifunctional hydroxy dicarboxylic acids of HDMGA (including dicarboxylic acid and one hydroxyl group), it may be logical to form hydrogen bonds with steady homo- and heteromolecular clusters, such as the bifunctional compounds of pinic, pinonic, and norpinic acids,[36] and they may participate in NPF and further growth processes.[2,13] In general, the occurrence of the compound in both laboratory and field measurements suggests that it may be an important SOA tracer, which needs further study. Taking into account the complexity and variability of the atmosphere, the specific nucleation mechanism of HDMGA cannot be clearly understood; therefore, theoretical calculations have been carried out to investigate its possible reactions in nucleation processes.

Amines[37–40] and organic acids[9] involved in atmospheric aerosol nucleation have been found in many field observations. When compared with monocarboxylic acids, dicarboxylic acids with lower saturation vapor pressures may participate in NPF.[41] Previous studies have shown the involvement of amines in NPF events.[37] In addition, for NPF, some evidences show that amines may play a key role in laboratory studies and field observations.[38–40] Dimethylamine (DMA), the most common and strongest organic base in air,[42,43] can react with different acids, which may be accompanied by proton transfer, enhancing reactions with other clusters. In experiments using the CLOUD chamber at CERN, the NPF rate of DMA with concentrations over 3 ppt is more than 3 orders of magnitude higher than that of ammonia.[40] Amines and dicarboxylic acids are likely to be involved in reactions at the molecular cluster levels.[44,45]

According to previous studies, DMA and HDMGA are involved in NPF events, but the mechanism of NPF, particularly the nucleation mechanism between HDMGA and DMA, has not been clearly understood. In this work, the possible ways of understanding ternary nucleation by HDMGA and DMA with water and binary nucleation by HDMGA with water are investigated. Topological analysis, temperature effect, hydration effect, and thermochemical analysis of different clusters containing HDMGA, DMA, and water are also explored.

2. Computational methods

The basin hopping (BH) algorithm[46–48] coupled with DFT were used to obtain the initial structures of $(HDMGA)(H_2O)_n$ (n = 0–3) and $(HDMGA)(DMA)(H_2O)_n$ (n = 0–3), a generalized gradient approximation in the Perdew–Burke–Ernzerhof (PBE) functional and the double numerical plus d-functions (DND) basis set implemented in the DMol[48] software package.[49] Our previous studies[50–57] have indicated that the BH method is appropriate for atomic and molecular systems.

To obtain the local minimum structures with the BH method, two steps need to be executed. Firstly, the initial configurations were obtained through the random displacement of atoms; then, the configurations were optimized to the local energy minima. Secondly, the optimized local energy minima were considered as the criteria to accept or reject the initial structure, which was controlled by the Boltzmann weight factor and temperature ranging from 1000 to 5000 K in this study.[58–61] Then, 30 initial lowest-energy geometries were selected to be optimized.[55,62] The initial geometries of $(HDMGA)(H_2O)_n$ (n = 0–3) and $(HDMGA)(DMA)(H_2O)_n$ (n = 0–3) were first optimized at the M06-2X/6-31++G(d,p) level. After that, the isomers located within 6 kcal mol^{-1} related to the global minimum were further optimized by the M06-2X/6-311++G(3df,3pd) level of theory to obtain the final geometries.[63,64] Performing simple optimization followed by fine optimization can save more time to obtain the final configurations than only using the M06-2X/6-311++G(3df,3pd) level of theory. To ensure that the final configurations do not eliminate the imaginary frequencies, frequency calculations were also performed. Equilibrium geometries and frequency calculations were carried out by the Gaussian09 program;[65] simultaneously, the thermochemistry of the clusters were obtained at 298.15 K and 1 atm.

Oxalic acid is a representative dicarboxylic acid that is widespread in the atmosphere, and our earlier benchmark work[66] involving oxalic acid and DMA clusters by using M06-2X, PW91PW91, and wB97X-D DFT functionals compared against the higher-level CCSD(T)-F12a/VDZ-F12 indicated M06-2X was suitable for $(C_2H_2O_4)_m(DMA)(H_2O)_n$ (m = 1–2, n = 0–4) systems. Jonas Elm *et al.*[67] indicated that the performance of the M06-2X functional using the 6-311++G(3df,3pd) basis set is excellent with regard to determining both geometries and energies than the traditional PW91 functional, at the same standard of experimental results. The M06-2X functional was selected owing to its good performance in estimating stable structures, thermochemistry, and noncovalent interactions (NCIs) for different atmospheric clusters[67–71] containing organic acids and showed good compromise in accuracy in comparison with computational cost.[72] The 6-311++G(3df,3pd) basis set was selected because it was widely used in atmospheric clusters.[73–81]

As compared to *ab initio* MP2 and higher-level methods, DFT is more suitable for investigating large clusters in view of the large computational cost; therefore, M06-2X/6-311++G(3df,3pd) was selected.[82]

3. Results and discussion

3.1 Structures

The geometries of (HDMGA)$(H_2O)_n$ (n = 0–3) and (HDMGA)-(DMA)$(H_2O)_n$ (n = 0–3) are optimized at the M06-2X/6-311++G(3df,3pd) level, and the global minimum structures are shown in Fig. 1 and 2, respectively. All the low-energy structures are listed in ESI.† In all the figures, the Gibbs free energies are ordered as a < b < c < d < e < f < g < h < i < j.

The notation m.n-i is used to represent different geometries, where m-1 and n are the notations for the different numbers of DMA and water molecules, respectively, and i is used to distinguish between various isomers with the same amount of HDMGA, DMA, and water. In order to distinguish between two carboxyl groups in HDMGA, the carboxyl attached to a single carbon atom is called the α-carboxyl group, and the carboxyl attached to a methylene is called a β-carboxyl group.

(HDMGA)$(H_2O)_n$ (n = 0–3). Fig. 1 shows the optimized global minima of HDMGA with 0–3 water molecules. For (HDMGA)$(H_2O)_1$ dimer, the water molecule bonds to α-carboxyl, forming the O···H hydrogen bond with a distance of 1.757 Å. For (HDMGA)$(H_2O)_2$, two water molecules and one HDMGA molecule form a three-membered ring with β-carboxyl. The three-membered ring is made up of three O···H hydrogen bonds, with successively increasing lengths of 1.640 Å, 1.740 Å, and 1.791 Å. When a third water molecule is added to HDMGA, there are four O···H hydrogen bonds in the lowest-energy configuration. The hydrogen bond with a length of 1.585 Å between the β-carboxyl and oxygen atom of water is the strongest than any other hydrogen bonds in the configuration. The second water molecule bonds to the hydrogen atom of the initial water with a length of 1.747 Å. The third water links with the second water and external hydroxyl, forming two O···H hydrogen bonds with distances of 1.762 Å and 1.933 Å. It is obvious that when the second or third water is added to HDMGA, β-carboxyl begins to form O···H hydrogen bonds instead of α-carboxyl, which may be caused by the space steric effect. In addition, for 1.2-a and 1.3-a, the strength of hydrogen bonds from the hydrogen atom of the β-carboxyl group to the end of the ring gradually weakens.

(HDMGA)(DMA)$(H_2O)_n$ (n = 1–3). When one DMA molecule is added to (HDMGA)$(H_2O)_n$ (n = 1–3), the optimized global minimum clusters are shown in Fig. 2. For the (HDMGA)(DMA) dimer, two kinds of hydrogen bonds exist: the intramolecular hydrogen bond formed between hydroxyl and α-carboxyl with the length of 1.994 Å, and the intermolecular hydrogen bond formed between the amino and carboxyl has a length of 1.611 Å. For (HDMGA)(DMA)$(H_2O)_1$, based on the cluster 2.0-a, two other new hydrogen bonds appear, forming a ring between the water molecule and β-carboxyl. It is obvious that the intramolecular hydrogen bond of 2.1-a with a length of 1.988 Å is stronger than that of 2.0-a; however, the intermolecular hydrogen bond of 2.1-a with a length of 1.621 Å is weaker than that of 2.0-a. For (HDMGA)(DMA)$(H_2O)_2$, proton transfer occurs from the oxygen atom of α-carboxyl to the nitrogen atom of the amino group, which indicates that water plays a crucial role in the proton transfer. The oxygen atom of α-carboxyl forms three hydrogen bonds. The first

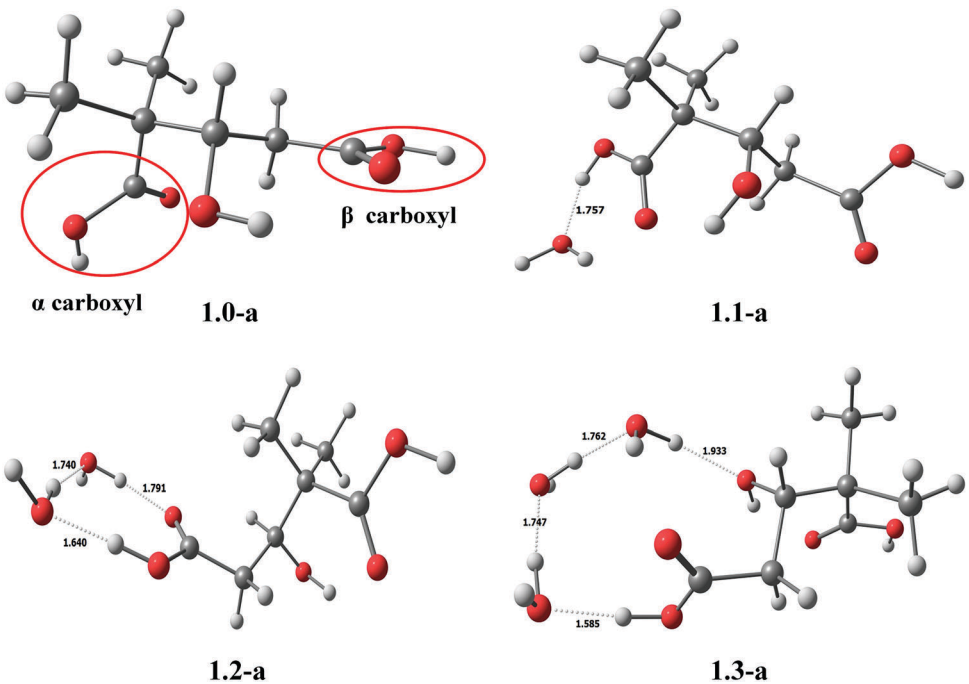

Fig. 1 Global minima of (HDMGA)$(H_2O)_n$ (n = 0–3) calculated at the M06-2X/6-311++G(3df,3pd) level.

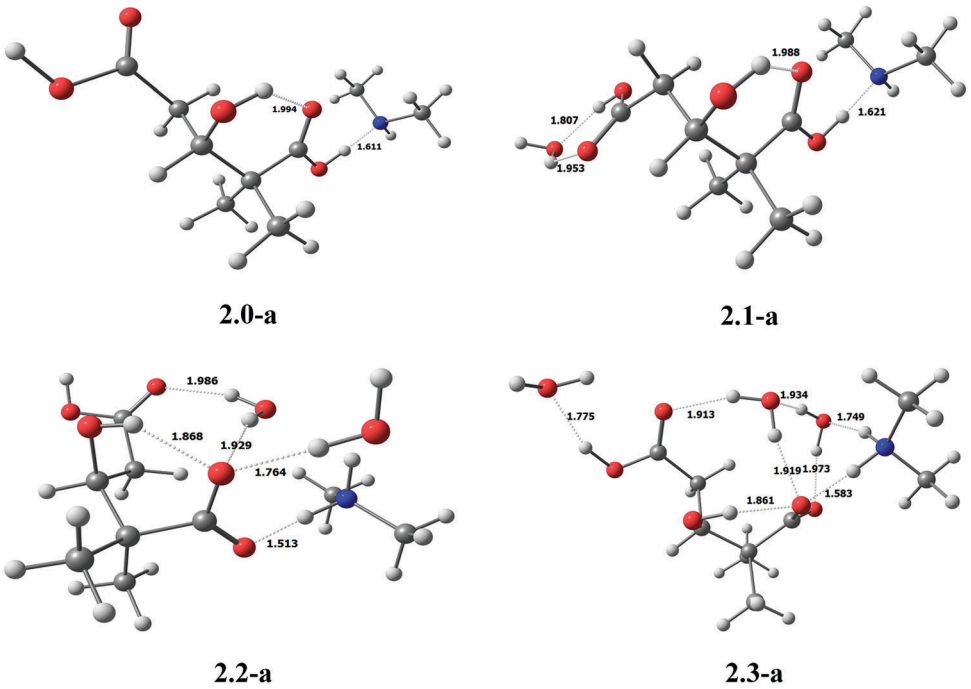

Fig. 2 Global minima of (HDMGA)(DMA)$(H_2O)_n$ (n = 0–3) calculated at the M06-2X/6-311++G(3df,3pd) level.

one is an intramolecular hydrogen bond, which connects α-carboxyl with hydroxyl. The second one connects to water, acting as a bridge between the two carboxyl groups. The third one, connected with a single water molecule, has the strongest hydrogen bond with a distance of 1.764 Å. For (HDMGA)(DMA)$(H_2O)_3$, all the hydrogen bonds make the cluster look like a cage. Proton transfer also occurs in this cluster with α-carboxyl as the donor and nitrogen atom as the acceptor.

In conclusion, adding a DMA molecule to (HDMGA)$(H_2O)_n$ (n = 1–3) promotes the formation of intramolecular hydrogen bonds, which imparts additional stability to the structure. Proton transfer is affected by the degree of hydration of (HDMGA)(DMA) clusters. When adding two or three water molecules, proton transfer takes place. In addition, α-carboxyl binds to DMA and forms an intramolecular hydrogen bond, which may be induced by the space steric effect.

3.2 Analysis of topological parameters

In this section, the topological parameters in the global minima of (HDMGA)(DMA)$(H_2O)_n$ (n = 0–3) will be discussed. As shown in Table 1, when the number of water molecules increases from 0 to 3, the length of H–N···H–O gets progressively shorter, except for n = 1; however, the deviation is marginal. It is obvious that when the second water is added to (HDMGA)(DMA)$(H_2O)_1$, the length of H–N···H–O exhibits a sharp decline. In order to further explore the nature of the hydrogen bonds on the stability of the global minimum structures, the "atoms in molecules" (AIM) theory of Bader is used to analyze the features at the bond critical points (BCPs) of N–H···O and O–H···O bonds.[83–87] The topological analysis of the electron density is an important part of AIM theory, which reveals the presence of the redistribution of electron density at the hydrogen bond.[88] The parameters at BCPs of N–H···O and O–H···O bonds are supported by topological analysis, including the electron density (ρ); Laplacian of electron density ($\Delta^2\rho$); and electronic energy density (H), which is the sum of the electronic kinetic energy density (G) and electronic potential energy density (V). All the topological parameters at the BCPs of N···H and O···H hydrogen bonds are presented in Tables 1 and 2, including the length of hydrogen bonds calculated at the M06-2X/6-311++G(3df,3pd) level. The topological analysis of the AIM theory was carried out by the Multiwfn program.[89]

Table 1 N···H distances (Å) and topological parameters at the intermolecular bond critical points (BCPs) of the N···H hydrogen bonds in the global minima of (HDMGA)(DMA)$(H_2O)_n$ (n = 0–3) calculated at the M06-2X/6-311++G(3df,3pd) level of theory

n	D(N···HO)/Å	ρ/a.u.	G/a.u.	V/a.u.	H/a.u.	$\Delta^2\rho$/a.u.	$-G/V$
0	1.611	0.0712	0.0408	−0.0701	−0.0293	0.0462	0.5820
1	1.621	0.0695	0.0402	−0.0683	−0.0281	0.0482	0.5886
2	1.089	0.2822	0.0486	−0.4912	−0.4427	−1.5763	0.0989
3	1.073	0.2965	0.0482	−0.5203	−0.4722	−1.6959	0.0926

Table 1 shows that as the number of water molecules increases up to two, the length of the H–N···H bond rapidly decreases from 1.621 Å to 1.089 Å. On the contrary, the electronic density sharply increases from 0.0695 a.u. to 0.2822 a.u., which means the strength of the hydrogen bond increases. The value of the electronic density at the BCPs indicates the strength of the interaction; in other words, the larger the electronic density, the stronger is the hydrogen bond.[90,91] Proton transfer occurs from the oxygen atom of the

α-carboxyl to the nitrogen atom of amino in (HDMGA)(DMA)$(H_2O)_2$; therefore, the second water may trigger proton transfer in the cluster. However, when the second water is added to (HDMGA)$(H_2O)_1$, no proton transfer occurs; therefore, DMA is essential for proton transfer.

The strength of the hydrogen bond is determined by the $\Delta^2\rho$ and H values. When both $\Delta^2\rho$ and H are positive, the hydrogen bond is weak. When $\Delta^2\rho$ is positive and H is negative, it is termed as a medium hydrogen bond. When both $\Delta^2\rho$ and H are negative, the hydrogen bond is strong.[87] The $\Delta^2\rho$ value is used to distinguish between covalent or NCI. In shared interactions, such as in a covalent bond, the $\Delta^2\rho$ value is negative. In closed-shell interactions, that is hydrogen bonds, ionic interactions, or van der Waals forces, the $\Delta^2\rho$ value is positive.[83] Therefore, these criteria are used to characterize different hydrogen bonds in the global minima of (HDMGA)(DMA)$(H_2O)_n$ (n = 0–3). For (HDMGA)(DMA) and (HDMGA)(DMA)$(H_2O)_1$ clusters, $\Delta^2\rho > 0$ and $H < 0$ suggest medium hydrogen bonds. For (HDMGA)(DMA)$(H_2O)_2$ and (HDMGA)(DMA)$(H_2O)_3$ clusters, both $\Delta^2\rho$ and H are negative, indicating strong hydrogen bonds in the closed-shell interactions, which mean hydrogen bonds transform into covalent interactions. It is consistent with the description of the structural section.

In contrast with intermolecular hydrogen bonds, the topological analyses of the intramolecular hydrogen bonds at O–H···O in HDMGA were also carried out, and the topological parameters at O–H···O of the global minima of (HDMGA)(DMA)$(H_2O)_n$ (n = 0–3) are shown in Table 2.

As the number of added water molecules increased from 0 to 3, the lengths of intramolecular hydrogen bonds at OH···O are 1.994 Å, 1.988 Å, 1.868 Å, and 1.861 Å, respectively. On the contrary, the electron densities are 0.0246 a.u., 0.0249 a.u., 0.0322 a.u., and 0.0327 a.u., respectively. The sudden increase in the electron density from 0.0249 a.u. to 0.0322 a.u. is probably attributed to the intermolecular proton transfer. For (HDMGA)(DMA) and (HDMGA)(DMA)$(H_2O)_1$ clusters, $\Delta^2\rho > 0$ and $H > 0$ indicate weak intramolecular hydrogen bonds. For (HDMGA)(DMA)$(H_2O)_2$ and (HDMGA)(DMA)$(H_2O)_3$, $\Delta^2\rho > 0$ and $H < 0$ indicate medium intramolecular hydrogen bonds. The changes from weak hydrogen bonds to strong hydrogen bonds are related to the proton transfer in (HDMGA)(DMA)$(H_2O)_2$. Proton transfer changes the electron density and enhances the strength of intramolecular hydrogen bonds. All the $\Delta^2\rho$ values at O–H···O in intramolecular hydrogen bonds are positive, indicating that the interactions are noncovalent.[92]

Table 2 O···H distances (Å) and topological parameters at the intramolecular BCPs of the O···H hydrogen bonds in the global minima of (HDMGA)(DMA)$(H_2O)_n$ (n = 0–3) calculated at the M06-2X/6-311++G(3df,3pd) level of theory

n	d(O···HO)/Å	ρ/a.u.	G/a.u.	V/a.u.	H/a.u.	$\Delta^2\rho$/a.u.	$-G/V$
0	1.994	0.0246	0.0229	−0.0211	0.1779×10^{-2}	0.0986	1.0853
1	1.988	0.0249	0.0233	−0.0215	0.1767×10^{-2}	0.1002	1.0837
2	1.868	0.0322	0.0294	−0.0295	-0.7426×10^{-4}	0.1173	0.9966
3	1.861	0.0327	0.0299	−0.0301	-0.2161×10^{-3}	0.1188	0.9934

In conclusion, as presented in Tables 1 and 2, the maximum length of the intermolecular hydrogen bond (1.621 Å) is shorter than the minimum length of the intramolecular hydrogen bond (1.861 Å). Therefore, the strength of the intermolecular hydrogen bonds is stronger than the intramolecular hydrogen bonds, that is, intermolecular hydrogen bonds are dominant in clusters. The dramatic increase in the electron density in the (HDMGA)(DMA)$(H_2O)_2$ cluster proves that proton transfer has occurred. The occurrence of proton transfer also enhances the strength of the intramolecular hydrogen bond.

3.3 Analysis of NCIs

Yang and coworkers[93] presented the NCI index based on the relationship between the reduced density gradient and electron density. The reduced density gradient (RDG), s, was calculated to represent the deviation from a homogeneous electron distribution.[94,95] As presented in eqn (1), ∇ is the gradient operator and $|\nabla\rho|$ is the electronic density gradient mode. According to previous studies, it is a useful approach to determine and visualize different kinds of NCIs in real space, such as hydrogen bonds and van der Waals forces. Therefore, the NCI index is used to investigate NCIs in (HDMGA)$(H_2O)_n$ (n = 1–3).

$$s = \frac{1}{2(3\pi^2)^{1/3}} \frac{|\nabla\rho|}{\rho^{4/3}} \quad (1)$$

The value of sign$(\lambda_2)\rho$ is an effective indicator of the strength of the interaction, which determines the color that is painted in the gradient isosurface.[93] When the value of sign$(\lambda_2)\rho$ is large and negative, the interaction forms a hydrogen bond; when the value of sign$(\lambda_2)\rho$ is close to zero, it means that the interaction is weak, such as van der Waals forces; when the value of sign$(\lambda_2)\rho$ is large and positive, the interaction is nonbonding. The gradient isosurfaces display a vivid visualization of the strength of NCIs, not just simple connections between atoms.

The plots of RDG (s) *vs.* electron density (ρ) multiplied by the sign of the second Hessian eigenvalue (λ_2) and corresponding isosurfaces for the global minima of (HDMGA)$(H_2O)_n$ (n = 1–3) are shown in Fig. 3, which are obtained by using the Multiwfn[89] and VMD[96] programs, respectively. The color of RDG (s) *vs.* sign$(\lambda_2)\rho$ and the isosurfaces have the same meaning; blue color represents hydrogen bonds; green, van der Waals forces; and red, steric hindrance. The darker the corresponding color, the stronger is the interaction. According to the isosurfaces, there are 1, 3, and 4 hydrogen bonds in (HDMGA)$(H_2O)_1$, (HDMGA)$(H_2O)_2$, and (HDMGA)$(H_2O)_3$, respectively. In the case of Fig. 3(b), the depth of the color is also consistent with the abovementioned strength of hydrogen bonds. From the hydrogen atom of the carboxyl to the oxygen atom of the carboxyl, the strength of the hydrogen bond gradually weakens, and the blue color gradually becomes lighter. In the case of Fig. 3(c), it is obvious that there are four hydrogen bonds from the hydrogen atom of the carboxyl to the oxygen atom of the hydroxyl, and the strength decreases, in turn, corresponding to the color of

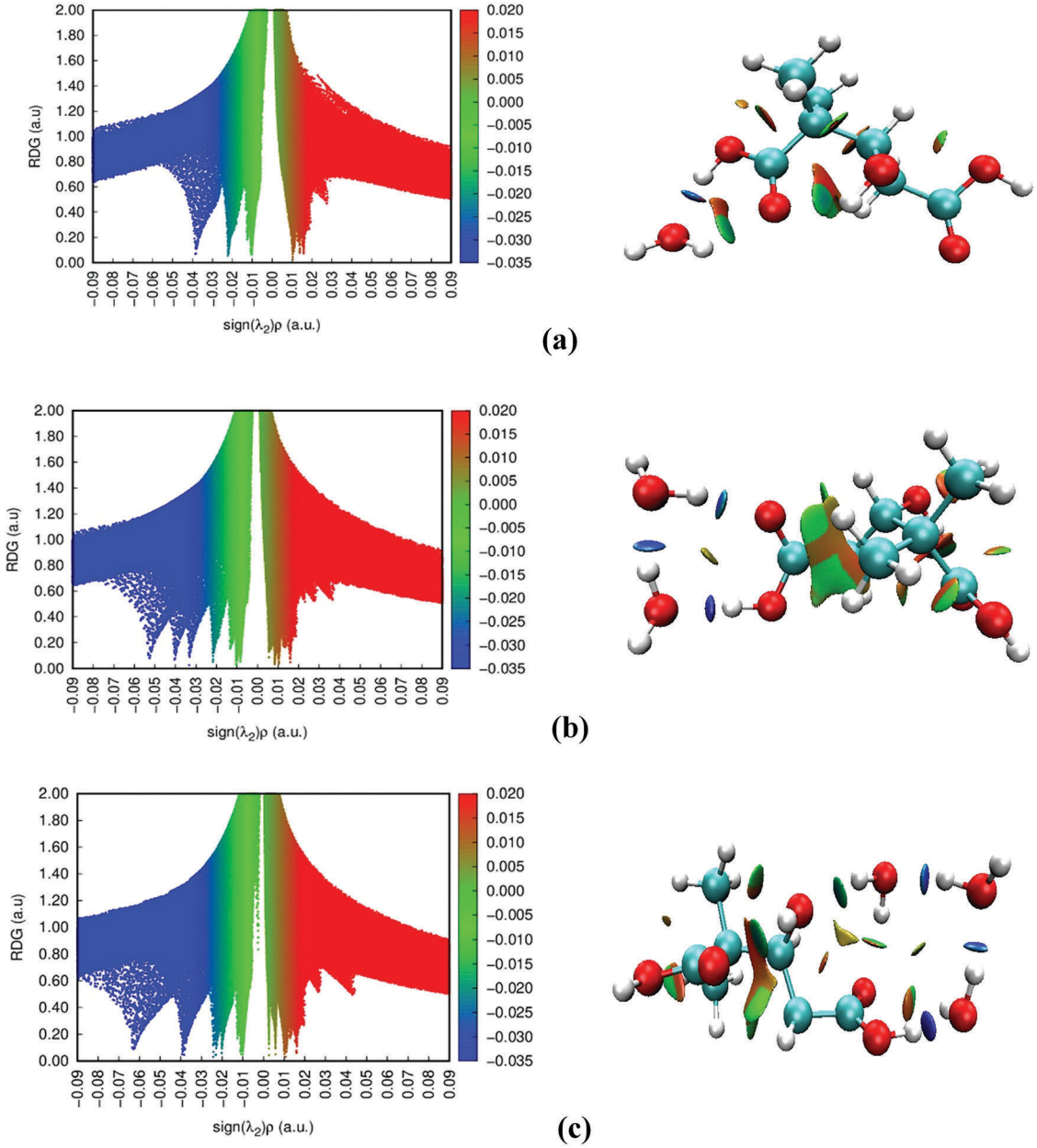

Fig. 3 Noncovalent interaction (NCI) analysis in the global minima of (HDMGA)$(H_2O)_n$ (n = 1–3) calculated at the M06-2X/6-311++G(3df,3pd) level.

RDG (s) *vs.* sign(λ_2)ρ map. All the results are consistent with those mentioned in the structural section.

3.4 Temperature dependence of conformational populations

As the temperature changes in the atmosphere, the thermodynamic properties of different configurations may change, which, in turn, affects the order of the conformational populations.[55,56] Therefore, it is necessary to investigate the temperature dependence of conformational populations including (HDMGA)$(H_2O)_n$ (n = 1–3) and (HDMGA)(DMA)$(H_2O)_n$ (n = 0–3). However, it is difficult to undertake experiments under low-temperature conditions because of the increasing wall losses of the clusters. Fortunately, theoretical calculations can predict the possible results. Fig. 4 shows the temperature dependence of (HDMGA)$(H_2O)_n$ (n = 1–3) and (HDMGA)(DMA)$(H_2O)_n$ (n = 0–3) at 100, 150, 200, 250, 298.15, and 300 K. In this study, W denotes water.

For the (HDMGA)$(H_2O)_1$ dimer, it is distinctly evident that the proportion of 1.1-a decreases from 55.6% to 38.8% in the range of 100–300 K. As a comparison, the proportion of 1.1-c increases from 11.6% to 22.5%. For (HDMGA)$(H_2O)_2$ (Fig. 4(b)), the proportion of 1.2-a steadily decreases from 85.5% to 54.8% in the range of 100–300 K. The isomers of 1.2-b, 1.2-c, and 1.2-d have similar trends. For (HDMGA)$(H_2O)_3$ (Fig. 4(c)), the most prevalent conformer is 1.3-a in the range of 100–300 K; the share of 1.3-a marginally decreases from 87.7% to 76.6%. The proportion of 1.3-b, which is the second stable isomer, is maintained at about 12% in the range of 100–300 K. The third

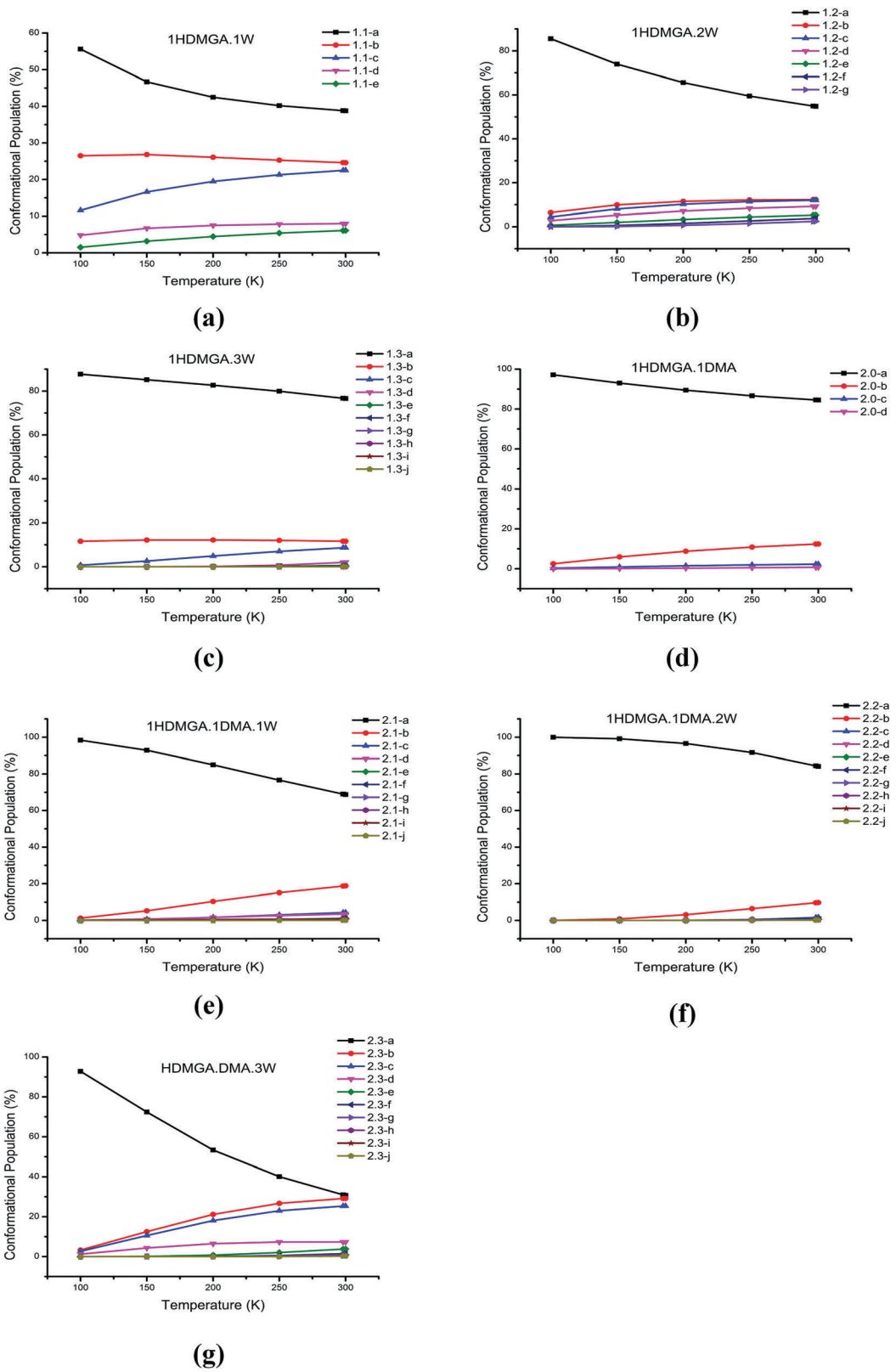

Fig. 4 Conformational population changes *vs.* temperature for the low-energy isomers of $(HDMGA)(H_2O)_n$ (n = 1–3) and $(HDMGA)(DMA)(H_2O)_n$ (n = 0–3) calculated at the M06-2X/6-311++G(3df,3pd) level.

stable isomer is 1.3-c, which shows a slightly increasing trend from 0.7% to 8.7%. Other isomers show negligible activity. When the temperature reaches 300 K, the proportions of 1.3-b and 1.3-c are approximately 11.6% and 8.7%, respectively.

For (HDMGA)(DMA)$(H_2O)_1$ (Fig. 4(e)), the proportion of the most stable structure steadily decreases from 98.4% to 68.7%; however, the proportion of the second stable structure steadily increases from 1.3% to 18.8% in the range of 100–300 K. For (HDMGA)(DMA)$(H_2O)_2$ (Fig. 4(f)), the most stable isomer, 2.2-a, has a proportion of approximately 100% in the range of 100–150 K; the presence of the other isomers is negligible in the atmosphere. However, when the temperature exceeds 150 K, the proportion of isomer 2.2-a decreases; at the same time, the proportion of 2.2-b gradually increases. At 300 K, 2.2-a still plays a dominant role with a proportion of 84.1%; 2.2-b only has a proportion of 9.8%, and the presence of other isomers is negligible. For (HDMGA)(DMA)$(H_2O)_3$ (Fig. 4(g)), the proportion of the global minimum isomer, 2.3-a, has a sharp decline from 92.8% to 30.7% in the range of 100–300 K. The second and third stable isomers, 2.3-b and 2.3-c, exhibit a similar trend: increasing from 3.3% to 29.2% and from 2.7% to 25.4%, respectively. There is a slight increase in the proportion of 2.3-d in the range of 100–300 K.

In conclusion, for (HDMGA)$(H_2O)_n$ (n = 1–3) and (HDMGA)(DMA)$(H_2O)_n$ (n = 0–3), it is obvious that the global minimum isomers of 1.1-a, 1.2-a, 1.3-a, 2.0-a, 2.1-a, 2.2-a, and 2.3-a are always dominant in the range of 100–300 K. However, for (HDMGA)(DMA)$(H_2O)_3$, 300 K may be a turning point, beyond which the proportion of 2.3-b and 2.3-c may exceed the most stable isomer, 2.3-a. In addition, when compared with Fig. 4(a) and (e), Fig. 4(b) and (f), and Fig. 4(c) and (g), when DMA was added, the stability of the global minimum clusters of (HDMGA)$(H_2O)_1$ and (HDMGA)$(H_2O)_2$ increased; however, the stability of the global minimum clusters of (HDMGA)$(H_2O)_3$ decreased. Therefore, DMA can promote the stability of hydration clusters to a certain extent. Fig. 4 shows that a change in the temperature affects the distribution of isomers, particularly for (HDMGA)(DMA)$(H_2O)_3$.

3.5 Thermochemical analysis

Studying the thermodynamic properties of different clusters can effectively reveal the possibility of clusters' formation in the atmosphere. Therefore, the thermodynamic analyses of the global minima in (HDMGA)$(H_2O)_n$ (n = 1–3) and (HDMGA)(DMA)$(H_2O)_n$ (n = 0–3) were carried out.

ΔE (0 K), ΔH (298.15 K), and ΔG (298.15 K) represent the relative single-point energies, enthalpies, and Gibbs free energy changes of the global minima between (HDMGA)$(H_2O)_n$ (n = 1–3) and (HDMGA)(DMA)$(H_2O)_n$ (n = 0–3) clusters, respectively. ΔE (0 K) is obtained by using two different reaction paths, as shown below. ΔE_1 is calculated by gradually adding a single H_2O molecule, and ΔE_2 is calculated by adding a cluster of $(H_2O)_n$. In addition, ΔH (298.15 K) and ΔG (298.15 K) are calculated in the same manner. The calculation results obtained in path 1 and path 2 are listed in Tables 3 and 4, respectively.

$$\Delta E_1 = E_{(\mathrm{HDMGA})(\mathrm{DMA})(\mathrm{H_2O})_n} - E_{(\mathrm{HDMGA})} - E_{(\mathrm{DMA})} - nE_{(\mathrm{H_2O})} \quad (2)$$

$$\Delta E_2 = E_{(\mathrm{HDMGA})(\mathrm{DMA})(\mathrm{H_2O})_n} - E_{(\mathrm{HDMGA})} - E_{(\mathrm{DMA})} - E_{((\mathrm{H_2O})_n)} \quad (3)$$

As presented in Table 3, all the ΔG values are negative, except for those of (HDMGA)$(H_2O)_1$ (0.02 kcal mol^{-1}), which implies that all the reactions can spontaneously occur, except for (HDMGA)$(H_2O)_1$. The ΔG value of (HDMGA)(DMA)$(H_2O)_1$ is −3.24 kcal mol^{-1}, which is −3.26 kcal mol^{-1} less than that in (HDMGA)$(H_2O)_1$. Further, the ΔG values of (HDMGA)(DMA)$(H_2O)_2$ and (HDMGA)$(H_2O)_2$ are −2.91 kcal mol^{-1} and −1.35 kcal mol^{-1}, respectively; therefore, the ΔG value of (HDMGA)(DMA)$(H_2O)_2$ is smaller than that of (HDMGA)$(H_2O)_2$ by about −1.56 kcal mol^{-1}. The ΔG value of (HDMGA)$(H_2O)_3$ (−1.10 kcal mol^{-1}) is smaller than that of (HDMGA)(DMA)$(H_2O)_3$ by about −2.23 kcal mol^{-1}. In addition, when HDMGA interacts with DMA, the change in the Gibbs free energy reaches the most negative value, which is −3.65 kcal mol^{-1}. The addition of DMA facilitates the progress of the reaction and increases the stability of the cluster, which is consistent with the findings of the structural and temperature correlation analyses.

As presented in Table 4, the ΔG values of (HDMGA)(DMA)$(H_2O)_2$, (HDMGA)$(H_2O)_2$, (HDMGA)(DMA)$(H_2O)_3$, and (HDMGA)$(H_2O)_3$ are −5.47 kcal mol^{-1}, −3.90 kcal mol^{-1}, −5.26 kcal mol^{-1}, and −4.14 kcal mol^{-1}, respectively, which is smaller than those calculated by path 1. The ΔE and ΔH values for (HDMGA)(DMA)$(H_2O)_2$, (HDMGA)$(H_2O)_2$, (HDMGA)(DMA)$(H_2O)_3$, and (HDMGA)$(H_2O)_3$ calculated by path 2 are larger than those calculated by path 1. When compared with path 1, all the ΔE and ΔH values calculated by path 2 are larger, while the ΔG values are smaller, which indicates that the process of adding a cluster of $(H_2O)_n$ is more likely in the atmosphere.

3.6 Atmospheric relevance

Previous studies[97,98] have shown that hydration is essential for the nucleation of amines and organic acids. The topological

Table 3 Thermodynamic properties calculated by gradually adding a single H_2O molecule in the formation of (HDMGA)$(H_2O)_n$ (n = 1–3) and (HDMGA)(DMA)$(H_2O)_n$ (n = 0–3) at the M06-2X/6-311++G(3df,3pd) level; the unit is kcal mol^{-1}

Reaction	ΔE (0 K)	ΔH (298.15 K)	ΔG (298.15 K)
HDMGA + H_2O ↔ (HDMGA)(H_2O)	−8.31	−8.74	0.02
HDMGA + $2H_2O$ ↔ (HDMGA)$(H_2O)_2$	−31.37	−19.28	−1.35
HDMGA + $3H_2O$ ↔ (HDMGA)$(H_2O)_3$	−27.10	−29.13	−1.10
HDMGA + DMA ↔ (HDMGA)(DMA)	−13.18	−12.90	−3.65
HDMGA + DMA + H_2O ↔ (HDMGA)(DMA)(H_2O)	−21.94	−22.46	−3.24
HDMGA + DMA + $2H_2O$ ↔ (HDMGA)(DMA)$(H_2O)_2$	−32.66	−34.06	−2.91
HDMGA + DMA + $3H_2O$ ↔ (HDMGA)(DMA)$(H_2O)_3$	−41.69	−44.12	−2.23

Table 4 Thermodynamic properties calculated by adding a cluster of $(H_2O)_n$ in the formation of $(HDMGA)(H_2O)_n$ (n = 1–3) and $(HDMGA)(DMA)(H_2O)_n$ (n = 0–3) at the M06-2X/6-311++G(3df,3pd) level; the unit is kcal mol^{-1}

Reaction	ΔE (0 K)	ΔH (298.15 K)	ΔG (298.15 K)
$HDMGA + H_2O \leftrightarrow (HDMGA)(H_2O)$	−8.31	−8.74	0.02
$HDMGA + (H_2O)_2 \leftrightarrow (HDMGA)(H_2O)_2$	−14.88	−15.58	−3.90
$HDMGA + (H_2O)_3 \leftrightarrow (HDMGA)(H_2O)_3$	−15.25	−15.37	−4.14
$HDMGA + DMA \leftrightarrow (HDMGA)(DMA)$	−13.18	−12.90	−3.65
$HDMGA + DMA + H_2O \leftrightarrow (HDMGA)(DMA)(H_2O)$	−21.94	−22.46	−3.24
$HDMGA + DMA + (H_2O)_2 \leftrightarrow (HDMGA)(DMA)(H_2O)_2$	−29.49	−30.35	−5.47
$HDMGA + DMA + (H_2O)_3 \leftrightarrow (HDMGA)(DMA)(H_2O)_3$	−29.85	−30.37	−5.26

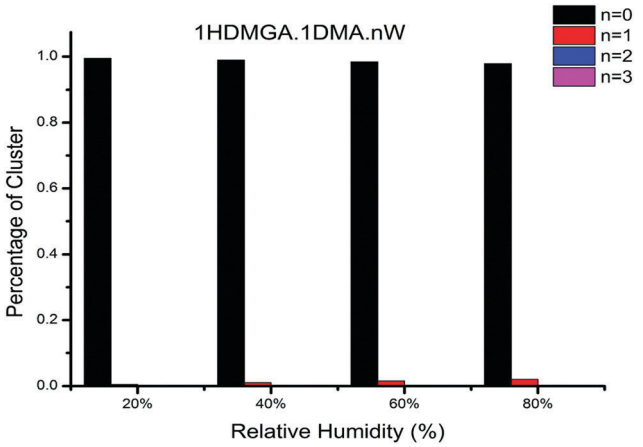

Fig. 5 Hydrate distributions of $(HDMGA)(DMA)(H_2O)_n$ (n = 0–3) clusters at the temperature of 298.15 K.

analysis of $(HDMGA)(DMA)(H_2O)_1$ shows that the addition of the second water triggers the proton transfer from HDMGA to DMA by generating ammonium dicarboxylate ion pairs. To determine the dominant cluster at a certain relative humidity (RH), the hydrate distributions of the "core" (HDMGA)(DMA) were calculated at various RHs at 298.15 K. The corresponding calculation methods have been given in our previous studies.[66,98]

The results of the hydrate distribution at four different RHs (20%, 40%, 60%, and 80%) are presented in Fig. 5. At RHs of 20%, 40%, 60%, and 80%, an unhydrated cluster is always dominant; however, dihydrate and trihydrate clusters do not exist. As the RH increases, the proportion of monohydrate clusters slightly increases from 0 to 2%. In conclusion, increasing the RH from 20% to 80% has a negligible effect on the hydrate distribution of (HDMGA)(DMA) clusters, and the unhydrated cluster is dominant all the time.

4. Conclusions

In this study, the nucleation mechanisms in the atmospheric NPF of $(HDMGA)(H_2O)_n$ (n = 1–3) and $(HDMGA)(DMA)(H_2O)_n$ (n = 0–3) are theoretically investigated by using the BH algorithm coupled with the DFT functional of the M06-2X/6-311++G(3df,3pd) level of theory. Structures, topological parameters, NCIs, temperature effect, hydration, and thermochemical analysis are explored.

The addition of DMA can promote the formation of intramolecular hydrogen bonds in HDMGA. The α-carboxyl group is directly attached to the amino group in all the most stable configurations, which may be caused by the space steric effect. When adding two or three water molecules, the clusters induce proton transfers from HDMGA to DMA. Such proton transfer enhances the strength of the hydrogen bond, as well as promotes the generation of a global minimum structure. The analysis of the electron density reveals that intermolecular hydrogen bonds play dominant roles as compared to intramolecular hydrogen bonds in $(HDMGA)(DMA)(H_2O)_n$ (n = 0–3).

Temperature has a considerable influence on the configuration distribution of isomers, particularly for $(HDMGA)(DMA)(H_2O)_3$. The Gibbs free energy values show that all the clusters under investigation exist in the process of nucleation, except for $(HDMGA)(H_2O)_1$, where (HDMGA)(DMA) is generated much more easily than the other dimer clusters. The process of adding a cluster of $(H_2O)_n$ more likely occurs in the atmosphere than gradually adding a single water molecule.

This work provides a readily available instrument to understand the nucleation mechanism of HDMGA and DMA. However, different problems still persist that need to be investigated. For example, whether HDMGA can react with other atmospheric compositions involving sulfuric acid or not. Further field observations, theoretical calculations, and experimental studies are necessary to investigate the possible reactions under atmospheric conditions.

Author contributions

Ya-Juan Han, Wei Huang and Ya-Juan Feng analyzed the results and wrote the manuscript. Shou-Kui Miao and Shuai Jiang prepared Fig. 1 and 2. Yi-Rong Liu, Chun-Yu Wang and Jiao Chen prepared Fig. 3–5. Zhong-Quan Wang, Teng Huang and Jie Li prepared Tables 1–4. All authors contributed to the manuscript.

Conflicts of interest

There are no conflicts to declare.

Acknowledgements

This work was supported by the National Natural Science Foundation of China (Grant No. 41775122, 21573241, 41605099,

41705097, 41705111, 41775112 and 41527808), the National Science Fund for Distinguished Young Scholars (Grant No. 41725019), Key Research Program of Frontier Science, CAS (Grant No. QYZDB-SSW-DQC031), The Key Research Program of the Chinese Academy of Sciences (Grant No. ZDRW-ZS-2016-4-3-6), the National Key Research and Development program (Grant No. 2016YFC0202203 and 2016YFC0202703) and National Research Program for Key Issues in Air Pollution Control (DQGG0103).

References

1 R. J. Charlson, S. E. Schwartz, J. M. Hales, R. D. Cess, J. A. Coakley, J. E. Hansen and D. J. Hofmann, *Science*, 1992, **255**, 423–430.
2 M. Kulmala, H. Vehkamaki, T. Petaja, M. Dal Maso, A. Lauri, V. M. Kerminen, W. Birmili and P. H. McMurry, *J. Aerosol Sci.*, 2004, **35**, 143–176.
3 G. Oberdörster and M. J. Utell, *Environ. Health Perspect.*, 2002, **110**, A440–A441.
4 J. Haywood and O. Boucher, *Rev. Geophys.*, 2000, **38**, 513–543.
5 F. Yu and G. Luo, *Atmos. Chem. Phys.*, 2009, **9**, 7691–7710.
6 J. Merikanto, D. V. Spracklen, G. W. Mann, S. J. Pickering and K. S. Carslaw, *Atmos. Chem. Phys.*, 2009, **9**, 8601–8616.
7 R. Y. Zhang, *Science*, 2010, **328**, 1366–1367.
8 L. Wang, A. F. Khalizov, J. Zheng, W. Xu, Y. Ma, V. Lal and R. Y. Zhang, *Nat. Geosci.*, 2010, **3**, 238–242.
9 R. Y. Zhang, A. Khalizov, L. Wang, M. Hu and W. Xu, *Chem. Rev.*, 2012, **112**, 1957–2011.
10 D. L. Yue, M. Hu, R. Y. Zhang, Z. B. Wang, J. Zheng, Z. J. Wu, A. Wiedensohler, L. Y. He, X. F. Huang and T. Zhu, *Atmos. Chem. Phys.*, 2010, **10**, 4953–4960.
11 B. Temelso, T. N. Phan and G. C. Shields, *J. Phys. Chem. A*, 2012, **116**, 9745–9758.
12 R. Y. Zhang, G. Wang, S. Guo, M. L. Zamora, Q. Ying, Y. Lin, W. Wang, M. Hu and Y. Wang, *Chem. Rev.*, 2015, **115**, 3803–3855.
13 M. Kulmala, *Science*, 2003, **302**, 1000–1001.
14 M. Claeys, B. Graham, G. Vas, W. Wang, R. Vermeylen, V. Pashynska, J. Cafmeyer, P. Guyon, M. O. Andreae, P. Artaxo and W. Maenhaut, *Science*, 2004, **303**, 1173–1176.
15 M. Jaoui, T. E. Kleindienst, M. Lewandowski, J. H. Offenberg and E. O. Edney, *Environ. Sci. Technol.*, 2005, **39**, 5661–5673.
16 M. Claeys, R. Szmigielski, I. Kourtchev, P. Van der Veken, R. Vermeylen, W. Maenhaut, M. Jaoui, T. E. Kleindienst, M. Lewandowski, J. H. Offenberg and E. O. Edney, *Environ. Sci. Technol.*, 2007, **41**, 1628–1634.
17 M. Hallquist, J. C. Wenger, U. Baltensperger, Y. Rudich, D. Simpson, M. Claeys, J. Dommen, N. M. Donahue, C. George, A. H. Goldstein, J. F. Hamilton, H. Herrmann, T. Hoffmann, Y. Iinuma, M. Jang, M. E. Jenkin, J. L. Jimenez, A. Kiendler-Scharr, W. Maenhaut, G. McFiggans, T. F. Mentel, A. Monod, A. S. H. Prevot, J. H. Seinfeld, J. D. Surratt, R. Szmigielski and J. Wildt, *Atmos. Chem. Phys.*, 2009, **9**, 5155–5236.
18 V. A. Lanz, M. R. Alfarra, U. Baltensperger, B. Buchmann, C. Hueglin, S. Szidat, M. N. Wehrli, L. Wacker, S. Weimer, A. Caseiro, H. Puxbaum and A. S. H. Prevot, *Environ. Sci. Technol.*, 2008, **42**, 214–220.
19 A. Guenther, C. N. Hewitt, D. Erickson, R. Fall, C. Geron, T. Graedel, P. Harley, L. Klinger, M. Lerdau, W. A. McKay, T. Pierce, B. Scholes, R. Steinbrecher, R. Tallamraju, J. Taylor and P. Zimmerman, *J. Geophys. Res.: Atmos.*, 1995, **100**, 8873–8892.
20 S. D. Piccot, J. J. Watson and J. W. Jones, *J. Geophys. Res.: Atmos.*, 1992, **97**, 9897–9912.
21 I. S. A. Isaksen and Ø. Hov, *Tellus B*, 1987, **39B**, 271–285.
22 H. J. I. Rinne, A. B. Guenther, J. P. Greenberg and P. C. Harley, *Atmos. Environ.*, 2002, **36**, 2421–2426.
23 A. Lee, H. Goldstein Allen, H. Kroll Jesse, L. Ng Nga, V. Varutbangkul, C. Flagan Richard and H. S. John, *J. Geophys. Res.: Atmos.*, 2006, **111**, D17305.
24 D. Hu, Q. Bian, W. Y. Li Teresa, K. H. Lau Alexis and Z. Y. Jian, *J. Geophys. Res.: Atmos.*, 2008, **113**, D22206.
25 T. E. Kleindienst, M. Jaoui, M. Lewandowski, J. H. Offenberg, C. W. Lewis, P. V. Bhave and E. O. Edney, *Atmos. Environ.*, 2007, **41**, 8288–8300.
26 M. Lewandowski, M. Jaoui, J. H. Offenberg, T. E. Kleindienst, E. O. Edney, R. J. Sheesley and J. J. Schauer, *Environ. Sci. Technol.*, 2008, **42**, 3303–3309.
27 P. Fu, K. Kawamura, J. Chen and L. A. Barrie, *Environ. Sci. Technol.*, 2009, **43**, 4022–4028.
28 B. R. Larsen, D. Di Bella, M. Glasius, R. Winterhalter, N. R. Jensen and J. Hjorth, *J. Atmos. Chem.*, 2001, **38**, 231–276.
29 A. Calogirou, B. R. Larsen and D. Kotzias, *Atmos. Environ.*, 1999, **33**, 1423–1439.
30 T. E. Kleindienst, M. Jaoui, M. Lewandowski, J. H. Offenberg, C. W. Lewis, P. V. Bhave and E. O. Edney, *Atmos. Environ.*, 2007, **41**, 8288–8300.
31 X. Ding, M. Zheng, L. Yu, X. Zhang, R. J. Weber, B. Yan, A. G. Russell, E. S. Edgerton and X. Wang, *Environ. Sci. Technol.*, 2008, **42**, 5171–5176.
32 I. Kourtchev, J. Warnke, W. Maenhaut, T. Hoffmann and M. Claeys, *Chemosphere*, 2008, **73**, 1308–1314.
33 P. A. Colin, D. O'Dowd, M. K. Kaarle Hämeri and T. Hoffmann, *Nature*, 2002, **416**, 497.
34 C. N. Shi, R. M. Yuan, B. W. Wu, Y. J. Meng, H. Zhang, H. Q. Zhang and Z. Q. Gong, *Sci. Total Environ.*, 2018, **642**, 1221–1232.
35 Q. H. Hu, Z. Q. Xie, X. M. Wang, H. Kang, Q. F. He and P. f. Zhang, *Sci. Rep.*, 2013, **3**, 2280.
36 T. Hoffmann, R. Bandur, U. Marggraf and M. Linscheid, *J. Geophys. Res.: Atmos.*, 1998, **103**, 25569–25578.
37 J. M. Mäkelä, S. Yli-Koivisto, V. Hiltunen, W. Seidl, E. Swietlicki, K. Teinilä, M. Sillanpää, I. K. Koponen, J. Paatero, K. Rosman and K. Hämeri, *Tellus B*, 2003, **53**, 380–393.
38 J. N. Smith, K. C. Barsanti, H. R. Friedli, M. Ehn, M. Kulmala, D. R. Collins, J. H. Scheckman, B. J. Williams and P. H. McMurry, *Proc. Natl. Acad. Sci. U. S. A.*, 2010, **107**, 6634–6639.

39 J. Zhao, J. N. Smith, F. L. Eisele, M. Chen, C. Kuang and P. H. McMurry, *Atmos. Chem. Phys.*, 2011, **11**, 10823–10836.
40 J. Almeida, S. Schobesberger, A. Kuerten, I. K. Ortega, O. Kupiainen-Maatta, A. P. Praplan, A. Adamov, A. Amorim, F. Bianchi, M. Breitenlechner, A. David, J. Dommen, N. M. Donahue, A. Downard, E. Dunne, J. Duplissy, S. Ehrhart, R. C. Flagan, A. Franchin, R. Guida, J. Hakala, A. Hansel, M. Heinritzi, H. Henschel, T. Jokinen, H. Junninen, M. Kajos, J. Kangasluoma, H. Keskinen, A. Kupc, T. Kurten, A. N. Kvashin, A. Laaksonen, K. Lehtipalo, M. Leiminger, J. Leppa, V. Loukonen, V. Makhmutov, S. Mathot, M. J. McGrath, T. Nieminen, T. Olenius, A. Onnela, T. Petaja, F. Riccobono, I. Riipinen, M. Rissanen, L. Rondo, T. Ruuskanen, F. D. Santos, N. Sarnela, S. Schallhart, R. Schnitzhofer, J. H. Seinfeld, M. Simon, M. Sipila, Y. Stozhkov, F. Stratmann, A. Tome, J. Troestl, G. Tsagkogeorgas, P. Vaattovaara, Y. Viisanen, A. Virtanen, A. Vrtala, P. E. Wagner, E. Weingartner, H. Wex, C. Williamson, D. Wimmer, P. Ye, T. Yli-Juuti, K. S. Carslaw, M. Kulmala, J. Curtius, U. Baltensperger, D. R. Worsnop, H. Vehkamaki and J. Kirkby, *Nature*, 2013, **502**, 359–363.
41 P. A. Makar, *Atmos. Environ.*, 2001, **35**, 961–974.
42 X. Ge, A. S. Wexler and S. L. Clegg, *Atmos. Environ.*, 2011, **45**, 561–577.
43 X. Ge, A. S. Wexler and S. L. Clegg, *Atmos. Environ.*, 2011, **45**, 524–546.
44 W. Xu and R. Y. Zhang, *J. Phys. Chem. A*, 2012, **116**, 4539–4550.
45 J. Zhao, A. Khalizov, R. Zhang and R. McGraw, *J. Phys. Chem. A*, 2009, **113**, 680–689.
46 J. W. Yoon, J. H. Park, C. C. Shur and S. B. Jung, *Microelectron. Eng.*, 2007, **84**, 2552–2557.
47 D. J. Wales and J. P. K. Doye, *J. Phys. Chem. A*, 1997, **101**, 5111–5116.
48 W. Huang, R. Pal, L. M. Wang, X. C. Zeng and L. S. Wang, *J. Chem. Phys.*, 2010, **132**, 054305.
49 B. Delley, *J. Chem. Phys.*, 1990, **92**, 508–517.
50 W. Huang, M. Ji, C. D. Dong, X. Gu, L. M. Wang, X. G. Gong and L. S. Wang, *ACS Nano*, 2008, **2**, 897–904.
51 W. Huang, A. P. Sergeeva, H. J. Zhai, B. B. Averkiev, L. S. Wang and A. I. Boldyrev, *Nat. Chem.*, 2010, **2**, 202–206.
52 L. L. Yan, Y. R. Liu, T. Huang, S. Jiang, H. Wen, Y. B. Gai, W. J. Zhang and W. Huang, *J. Chem. Phys.*, 2013, **139**, 244312.
53 S. Jiang, Y. R. Liu, T. Huang, H. Wen, K. M. Xu, W. X. Zhao, W. J. Zhang and W. Huang, *J. Comput. Chem.*, 2014, **35**, 159–165.
54 K. M. Xu, T. Huang, H. Wen, Y. R. Liu, Y. B. Gai, W. J. Zhang and W. Huang, *RSC Adv.*, 2013, **3**, 24492–24502.
55 Y. R. Liu, H. Wen, T. Huang, X. X. Lin, Y. B. Gai, C. J. Hu, W. J. Zhang and W. Huang, *J. Phys. Chem. A*, 2014, **118**, 508–516.
56 S. K. Miao, S. Jiang, J. Chen, Y. Ma, Y. P. Zhu, Y. Wen, M. M. Zhang and W. Huang, *RSC Adv.*, 2015, **5**, 48638–48646.
57 J. Chen, S. Jiang, S. K. Miao, X. Q. Peng, Y. Ma, C. Y. Wang, M. M. Zhang, Y. R. Liu and W. Huang, *RSC Adv.*, 2015, **5**, 91500–91515.
58 X. Chen, Y. F. Zhao, L. S. Wang and J. Li, *Comput. Theor. Chem.*, 2017, **1107**, 57–65.
59 Y. F. Zhao, X. Chen and J. Li, *Nano Res.*, 2017, **10**, 3407–3420.
60 S. Jiang, T. Huang, Y. R. Liu, K. M. Xu, Y. Zhang, Y. Z. Lv and W. Huang, *Phys. Chem. Chem. Phys.*, 2014, **16**, 19241–19249.
61 D. J. Wales and J. P. K. Doye, *J. Phys. Chem. A*, 1997, **101**, 5111–5116.
62 H. Wen, T. Huang, C. Y. Wang, X. Q. Peng, S. Jiang, Y. R. Liu and W. Huang, *Atmos. Environ.*, 2018, **191**, 214–226.
63 X. Q. Peng, Y. R. Liu, T. Huang, S. Jiang and W. Huang, *Phys. Chem. Chem. Phys.*, 2015, **17**, 9552–9563.
64 C. Y. Wang, S. Jiang, Y. R. Liu, H. Wen, Z. Q. Wang, Y. J. Han, T. Huang and W. Huang, *J. Phys. Chem. A*, 2018, **122**, 3470–3479.
65 G. T. M. Frisch, H. B. Schlegel, G. Scuseria, M. Robb, J. Cheeseman, G. Scalmani, V. Barone, B. Mennucci and G. Petersson, *Gaussian 09, Revision A.02*, Wallingford, CT, 2009, vol. 270, p. 271.
66 J. Chen, S. Jiang, Y. R. Liu, T. Huang, C. Y. Wang, S. K. Miao, Z. Q. Wang, Y. Zhang and W. Huang, *RSC Adv.*, 2017, **7**, 6374–6388.
67 J. Elm, M. Bilde and K. V. Mikkelsen, *J. Chem. Theory Comput.*, 2012, **8**, 2071–2077.
68 N. Bork, L. Du, H. Reiman, T. Kurtén and H. G. Kjaergaard, *J. Phys. Chem. A*, 2014, **118**, 5316–5322.
69 Y. Zhao and D. G. Truhlar, *Theor. Chem. Acc.*, 2008, **120**, 215–241.
70 L. Liu, X. Zhang, Z. Li, Y. Zhang and M. Ge, *Chemosphere*, 2017, **186**, 430–437.
71 J. Elm and K. Kristensen, *Phys. Chem. Chem. Phys.*, 2017, **19**, 1122–1133.
72 H. R. Leverentz, J. I. Siepmann, D. G. Truhlar, V. Loukonen and H. Vehkamäki, *J. Phys. Chem. A*, 2013, **117**, 3819–3825.
73 J. Herb, A. B. Nadykto and F. Yu, *Chem. Phys. Lett.*, 2011, **518**, 7–14.
74 B. A. Nadykto, F. Yu, V. M. Jakovleva, J. Herb and Y. Xu, *Entropy*, 2011, **13**, 554–569.
75 A. B. Nadykto, F. Yu and J. Herb, *Atmos. Chem. Phys.*, 2009, **9**, 4031–4038.
76 J. Herb, Y. Xu, F. Yu and A. B. Nadykto, *J. Phys. Chem. A*, 2013, **117**, 133–152.
77 B. A. Nadykto, F. Yu and J. Herb, *Int. J. Mol. Sci.*, 2008, **9**, 2184–2193.
78 A. B. Nadykto, F. Yu and J. Herb, *Chem. Phys.*, 2009, **360**, 67–73.
79 A. B. Nadykto and F. Yu, *Chem. Phys. Lett.*, 2007, **435**, 14–18.
80 Y. Xu, A. B. Nadykto, F. Yu, L. Jiang and W. Wang, *THEOCHEM*, 2010, **951**, 28–33.
81 Y. Xu, A. B. Nadykto, F. Yu, J. Herb and W. Wang, *J. Phys. Chem. A*, 2010, **114**, 387–396.
82 D. B. Cook, *Handbook of Computational Quantum Chemistry*, Oxford University Press, USA, 1998.
83 R. F. W. Bader, *Atoms in Molecules: A Quantum Theory*, Oxford University Press, *UK*, 1990.
84 M. T. Carroll, C. Chang and R. F. W. Bader, *Mol. Phys.*, 1988, **63**, 387–405.

85 W. Gao, J. q. Jiao, H. j. Feng, X. p. Xuan and L. p. Chen, *J. Mol. Model.*, 2013, **19**, 1273–1283.
86 R. G. A. Bone and R. F. W. Bader, *J. Phys. Chem.*, 1996, **100**, 10892–10911.
87 I. Rozas, I. Alkorta and J. Elguero, *J. Am. Chem. Soc.*, 2000, **122**, 11154–11161.
88 P. L. H. Popelier, *Atoms in Molecules: An Introduction*, Prentice Hall, London, 2000.
89 T. Lu, *Multiwfn Program, Version 3.5.*, 2018, http://sobereva.com/multiwfn/.
90 O. Galvez, P. C. Gomez and L. F. Pacios, *J. Chem. Phys.*, 2003, **118**, 4878–4895.
91 P. Politzer, J. S. Murray and T. Clark, *Phys. Chem. Chem. Phys.*, 2010, **12**, 7748–7757.
92 N. Han, Y. Zeng, X. Li, S. Zheng and L. Meng, *J. Phys. Chem. A*, 2013, **117**, 12959–12968.
93 E. R. Johnson, S. Keinan, P. Mori-Sánchez, J. Contreras-García, A. J. Cohen and W. Yang, *J. Am. Chem. Soc.*, 2010, **132**, 6498–6506.
94 P. Hohenberg and W. Kohn, *Phys. Rev.*, 1964, **136**, B864.
95 A. J. Cohen, P. Mori-Sánchez and W. Yang, *Science*, 2008, **321**, 792–794.
96 W. Humphrey, A. Dalke and K. Schulten, *J. Mol. Graphics*, 1996, **14**, 33–38.
97 W. Xu and R. Y. Zhang, *J. Chem. Phys.*, 2013, **139**, 11.
98 X. Q. Peng, T. Huang, S. K. Miao, J. Chen, H. Wen, Y. J. Feng, Y. Hong, C. Y. Wang and W. Huang, *RSC Adv.*, 2016, **6**, 46582–46593.